ADAMTS metalloproteases generate active versican fragments that regulate interdigital web regression

Daniel R. McCulloch[1], **Courtney M. Nelson**[1], **Laura J. Dixon**[1], **Debra L. Silver**[2], **James D. Wylie**[1], **Volkhard Lindner**[3], **Takako Sasaki**[4], **Marion A. Cooley**[5], **W. Scott Argraves**[5], and **Suneel S. Apte**[1],*

[1]Department of Biomedical Engineering, Cleveland Clinic, Cleveland, OH

[2]Genetic Disease Research Branch, National Human Genome Research Institute, Bethesda, MD, USA

[3]Maine Medical Center Research Institute, Scarborough, ME

[4]Department of Biochemistry and Molecular Biology, Oregon Health & Science University, Portland, OR

[5]Department of Anatomy and Cell Biology, Medical University of South Carolina, Charleston, SC.

Abstract

We show that combinatorial mouse alleles for the secreted metalloproteases *Adamts5*, *Adamts20* (*bt*), and *Adamts9* result in fully penetrant soft-tissue syndactyly. Interdigital webs in *Adamts5−/−; bt/bt* mice had reduced apoptosis and decreased cleavage of the proteoglycan versican; however, the BMP-FGF axis, which regulates interdigital apoptosis was unaffected. BMP4 induced apoptosis, but without concomitant versican proteolysis. Haploinsufficiency of either *Vcan* or *Fbln1*, a co-factor for versican processing by ADAMTS5, led to highly penetrant syndactyly in *bt* mice, suggesting that cleaved versican was essential for web regression. The local application of an amino-terminal versican fragment corresponding to ADAMTS-processed versican, induced cell death in *Adamts5−/−; bt/bt* webs. Thus, ADAMTS proteases cooperatively maintain versican proteolysis above a required threshold to create a permissive environment for apoptosis. The data highlight the developmental significance of proteolytic action on the ECM, not only as a clearance mechanism, but also as a means to generate bioactive versican fragments.

Keywords

Limb development; Interdigital web; Morphogenesis; Extracellular matrix; Proteoglycan; ADAMTS; Syndactyly; Apoptosis; Versican; Fibulin

*Corresponding Author: Suneel S. Apte, ND20-Cleveland Clinic, 9500 Euclid Avenue, Cleveland, Ohio 44195, USA **Tel:** 216 445 3278 **Fax:** 216 444 9198 aptes@ccf.org.

Nomenclature: *Adamts*# indicates the mouse genes, ADAMTS# indicates the corresponding protein.

INTRODUCTION

Classic examples of tissue sculpting during morphogenesis include resorption of tadpole tails and fins during amphibian metamorphosis (Gross and Lapiere, 1962) and regression of the interdigital webs during mammalian limb morphogenesis (Zuzarte-Luis and Hurle, 2002). Web regression is highly regulated, since interdigital tissue (IDT) provides cues for precise development of the skeletal elements of the autopod (Dahn and Fallon, 2000). Persistence of IDT leads to soft-tissue syndactyly (STS) in which only web resorption is affected, and is distinct from osseous syndactyly, where the skeletal elements of adjacent rays are fused owing to anomalous patterning earlier in development. STS is a relatively common developmental anomaly, occurring either in isolation or in association with other defects.

Web regression requires removal of interdigital cells, which occurs by apoptosis, as well as clearance of extracellular matrix (ECM). A complex interplay between BMPs and FGFs mediates apoptosis during IDT regression. During early mouse autopod development, FGFs produced in the apical ectodermal ridge (AER) promote outgrowth and suppress BMP production in the prospective IDT (Boulet et al., 2004; Lu et al., 2006; Weatherbee et al., 2006). BMPs also appear to regulate FGFs, which then act as survival factors for IDT cells (Pajni-Underwood et al., 2007). Once autopod patterning is complete, the AER regresses, FGF production in the AER declines, and BMP expression in the IDT is upregulated, leading to apoptosis of interdigital cells (Ganan et al., 1996; Guha et al., 2002; Merino et al., 1999a; Merino et al., 1999b; Weatherbee et al., 2006). STS is observed in *Bmp* deficient mice (Bandyopadhyay et al., 2006) and can be induced by the presence of the BMP inhibitor Gremlin (Merino et al., 1999b). Gremlin expression in the bat forelimb and duck hindlimb IDT may be a mechanism that ensures web retention and allows the formation of wings and webbed feet respectively (Weatherbee et al., 2006; Zou and Niswander, 1996).

In contrast to extensive published work on apoptosis during interdigital web regression, mechanisms for removal of the web ECM have not been previously identified, nor is it understood how synchronous removal of cells and ECM is achieved. During amphibian metamorphosis, the redundant tissues are collagen-rich, and induction of a secreted collagenase, which was incidentally the first discovered matrix-degrading metalloprotease, is necessary (Gross and Lapiere, 1962). However, IDT has an embryonic matrix, containing hyaluronan, proteoglycans and fibronectin, and collagenase is unlikely to have a major role in its regression. Here, we show that combinations of null alleles for three ADAMTS proteases (*Adamts5, Adamts9* and *Adamts20 (bt)*) lead to STS, but do not affect skeletal patterning, indicating a temporally and spatially restricted role during web regression. These ADAMTS proteases belong to an evolutionarily-related cluster of secreted metalloproteases that share the ability to cleave large aggregating chondroitin-sulfate proteoglycans (Apte, 2009). One such substrate is versican, a widespread embryonic proteoglycan, which forms complexes with hyaluronan through its N-terminal G1 domain (Kimata et al., 1986; Matsumoto et al., 2003) and interacts with several other molecules, including fibulin-1 (Aspberg et al., 1999), through its C-terminal G3 domain. Our findings reveal an operational model in which these ADAMTS proteases work cooperatively to influence apoptosis during web regression through the production of cleaved versican.

RESULTS

Adamts5−/−; bt/bt mice develop STS with greater penetrance than *Adamts5−/−* or *bt/bt* mice

In the course of investigating genes that could modify a white spotting defect in ADAMTS20-deficient *bt* mice (Silver, 2008), we found that *Adamts5−/−; bt/bt* mice developed syndactyly with 100 % penetrance (Fig. 1A). In contrast, *Adamts5−/−* mice and *bt/bt* mice each had a considerably lower penetrance of syndactyly (44% and 18% respectively). Penetrance in

combinatorial mice was dependent on the dosage of the mutant alleles (Fig. 1A). While at least 3 of 4 limbs were involved in each *Adamts5−/−; bt/bt* mouse (Supplemental Fig. S1), the severity and extent of fusion varied (Fig. 1B). The IDT between hindlimb digits 3 and 4 was most frequently involved in *Adamts5−/−; bt/bt* mice (Supplemental Fig. S2A) and also had the greatest severity of STS (Supplemental Fig. S2B). Hindlimbs were more frequently affected in *Adamts5−/−* mice, whereas forelimbs were more frequently affected in *bt/bt* mice (Supplemental Fig. S2C). 3-D reconstruction of limbs from mature *Adamts5−/−; bt/bt* mice using micro-computed tomography (mCT) showed that osseous syndactyly or patterning defects were absent (Fig. 1C). Thus, these proteases act locally in the IDT after completion of limb patterning.

Since ADAMTS20 is homologous to ADAMTS9 (Llamazares et al., 2003; Somerville et al., 2003), we tested whether *Adamts9* participated in IDT resorption. *Adamts9−/−* mice die during early gestation (Somerville, R.P.T., Apte, S.S., unpublished data); hence, *Adamts5−/−; Adamts9+/−* mice and *bt/bt; Adamts9+/−* mice were analyzed. We had previously identified cooperative developmental functions for *Adamts9* and *Adamts20* in *Adamts9+/−; bt/bt* mice, which have more extensive white spotting (Silver, 2008) as well as cleft palate, a phenotype absent in mice with either mutation alone (Enomoto, H., Nelson, C., Apte, S.S, manuscript in preparation). *Adamts5−/−; Adamts9+/−* mice had a considerably higher penetrance of syndactyly (87%) than either *Adamts5−/−* (44%) or *Adamts9+/−* mice, which did not develop syndactyly (Fig. 1A). They resembled *Adamts5−/−; bt/bt* mice, despite retaining one intact *Adamts9* allele. *Bt/bt; Adamts9+/−* mice, which were analyzed at 16.5 days of gestation owing to perinatal lethality from cleft palate, had completely penetrant STS. *Adamts5−/−; bt/+; Adamts9+/−* mice also had fully penetrant STS (Fig. 1A), as well as more affected limbs than *Adamts5−/−; Adamts9+/−* or *bt/bt; Adamts9+/−* mice (Supplemental Fig. S1). Thus, the allele dosage of these ADAMTS genes is important, and suggests a cooperative mode of action, with ADAMTS5 occupying a key position in IDT regression.

Adamts5, Adamts9 and *Adamts20* are co-expressed in IDT during web regression

The temporal restriction of the observed effects of combinatorial *Adamts* allele deletion during IDT regression suggested that these genes were coordinately expressed locally during this process. Accordingly, we determined their mRNA expression patterns during limb development. For *Adamts5*, we previously identified strong perichondrial expression at E14.5 using in situ hybridization (McCulloch et al., 2009). β-gal staining was used as a surrogate for *Adamts5* mRNA using an intragenic IRES-*lacZ* cassette (McCulloch et al., 2009), *in situ* hybridization was utilized for *Adamts20,* and both β-gal staining and *in situ* hybridization were used for *Adamts9*. All aspects of forelimb development anticipate the hindlimb by 0.5-1 day, and similar patterns were seen for each gene in forelimbs and hindlimbs within this chronologic gap. The distal limb lacked significant expression of these *Adamts* genes until E12.5 (*Adamts20*) or E13.5 (*Adamts5, Adamts9*). At E11.5, *Adamts5* was expressed in peripheral nerves entering the limb buds, *Adamts9* was expressed in core mesenchyme of the limb-buds, and *Adamts20* was diffusely present in both fore- and hind-limbs (Fig. 2A-C). From E13.5-E15.5, there was strong β-gal staining representing *Adamts5* mRNA in the perichondrium of the digit cartilages and IDT (Fig. 2A). *Adamts9* mRNA distribution, identified both by β-gal staining (Fig 2B) and *in situ* hybridization (Supplemental Fig. S3) overlapped considerably with *Adamts5* in the perichondrium of developing digit cartilages and IDT. At E13.5, *Adamts20* expression was seen in IDT and in the medial border of the autopod (Fig. 2C).

We also analyzed expression of *Adamts4,* which encodes a potent proteoglycan-degrading enzyme (Arner et al., 1999; Sandy et al., 2001) utilizing an intragenic IRES-lacZ reporter in *Adamts4−/−* mice, which showed very weak staining in the IDT at E13.5 and E14.5 (Fig. 2D and data not shown) and undetectable mRNA expression by RT-PCR (Fig. 2E). *Adamts4−/−*

mice did not develop STS. *Adamts4−/−; Adamts5−/−* mice and *Adamts4−/−; bt/bt* mice did not have greater penetrance or severity of STS than in the respective single deletions (data not shown). Previous work demonstrated prominent expression of *Adamts1* in IDT from E12.5-E15.5, similar to that described here for *Adamts5* and *Adamts9* (Thai and Iruela-Arispe, 2002). RT-PCR for the entire subset of proteoglycan-degrading ADAMTS proteases using E13.5 hindlimb autopod RNA (Fig. 2E), demonstrated expression of *Adamts15*, but not *Adamts8* in addition to the genes described above.

IDT in *Adamts5−/−; bt/bt* autopods have reduced apoptosis

Subsequent mechanistic analysis of STS was undertaken in *Adamts5−/−; bt/bt* mice. Since interdigit cells die during digit separation, we evaluated apoptosis in these mice. TUNEL-stained E14.5 *Adamts5−/−; bt/bt* hindlimb sections showed reduced apoptosis compared to wild-type controls (Fig. 3A). E14.5 autopods were also stained with acridine orange, which identifies apoptotic nuclei (Salas-Vidal et al., 2001), and staining in each interdigital space was scored in a blinded fashion (Fig 3 B,C). For this analysis, we used littermate *Adamts5−/−*; *bt/+* embryos as controls, since STS is markedly reduced by the presence of a wild-type (*wt*) *Adamts20* allele (Fig. 1A). Stained nuclei were less abundant in the *Adamts5−/−; bt/bt* limbs, with decreased staining being most evident in IDT between digits 2 and 3 and between digits 3 and 4 of the hindlimbs (Fig. 3C), consistent with the highest severity in these webs (Supplemental Fig. S2A, B).

The *Bmp-Fgf* axis is unaffected in *Adamts5−/−; bt/bt* autopods

BMPs are key mediators of IDT apoptosis and Gremlin antagonizes BMP signaling during IDT resorption (Bandyopadhyay et al., 2006; Guha et al., 2002; Merino et al., 1999a; Weatherbee et al., 2006). *Bmp2*, *Bmp4, Bmp7* and *Gremlin* expression were localized to the IDT, consistent with their role in local signaling, but their expression pattern was essentially similar in *Adamts5−/−; bt/bt* mice and control autopods (Fig. 3D). These data suggest that ADAMTS proteases do not act upstream of *Bmps* or *Gremlin*. Co-expression of Gremlin protein with ADAMTS5 in HEK293F cells showed no cleavage of Gremlin, suggesting that it is not degraded by ADAMTS5 (data not shown). Thus, lack of web resorption in *Adamts5−/−; bt/bt* mice could not be explained by defective BMP expression or by altered levels of the major BMP inhibitor, Gremlin, acting in the IDT. Expression of key BMP targets, *Msx1* and *Msx2* was unaltered (Fig. 3D). *Fgf4* and *Fgf8* were strongly expressed in an overlapping pattern with BMP genes although there was no difference between *Adamts5−/−; bt/bt* mice and wild-type control autopods (Fig. 3D). Intense expression of these FGFs in IDT was unexpected; insofar as we are aware, their expression has not been previously reported at this gestational age in the limbs and suggests a dramatic shift from the AER to IDT at E13.5. Immunostaining with an antibody that detects pSmad1/5/8 showed positively stained nuclei in the interdigit cells (Fig. 3E), and suggested that intracellular BMP signaling was unaffected in *Adamts5−/−; bt/bt* mice, consistent with normal *Msx1* and *Msx2* expression (Fig. 3D).

Cleavage of versican is reduced in *Adamts5−/−; bt/bt* autopods

Since web regression requires clearance of ECM as well as cells, we asked whether removal of ECM was affected in *Adamts5−/−; bt/bt* mice. Histology of *Adamts5−/−; bt/bt* autopods at E16.5, by which time the process of resorption is completed, demonstrated persistence of the IDT with a low cell density and loose, amorphous matrix, suggestive of high proteoglycan content (Fig. 4A, left and center panels). Immunohistochemistry demonstrated strong versican staining in this unabsorbed tissue (Fig. 4A, right-hand panel). Each of the three relevant ADAMTS proteases, as well as ADAMTS1 and ADAMTS4 can generate a specific C-terminal neo-epitope (DPEAAE) upon cleavage of the versican V1 isoform at the Glu^{441}-Ala^{442} peptide bond, that is recognizable either by specific staining on immunohistochemistry, or as a 70 kDa

band on western blots (Longpre et al., 2009;Sandy et al., 2001; Silver, 2008; Somerville et al., 2003). Anti-DPEAAE immunohistochemistry showed that cleaved versican was indeed present in the interdigital webs of wild-type mice (Fig. 4B, left-hand panel), whereas it was markedly reduced or absent in *Adamts5−/−; bt/bt* IDT (Fig 4B, right-hand panel). In contrast, no difference in the distribution of fibronectin, a widely-distributed embryonic ECM component, was observed (data not shown).

Because both reduced versican clearance and reduced apoptosis were present in *Adamts5−/−; bt/bt* IDT, we asked whether versican proteolysis was causally involved in regulation of apoptosis *via* a genetic approach in which we reduced the versican level in *bt* mice. Since lethality of the *Vcan* mutant mouse *hdf* (*heart defect*) (Mjaatvedt et al., 1998) occurs prior to IDT regression, versican cannot be completely deleted in *Adamts* deficient mice. Therefore, we introduced *Vcan* haploinsufficiency in *bt* mice i.e., we asked if a reduced versican burden could be effectively cleared, and apoptosis could be restored despite the reduced overall level of versican-degrading activity resulting from the absence of ADAMTS20. Unexpectedly, *bt/bt; hdf/+* mice had 100% penetrance of syndactyly, similar to *Adamts5−/−; bt/bt* mice, and considerably greater than that observed in either *bt/bt* or *Adamts5−/−* mice (Fig. 4C, Supplemental Figure S4). This genetic interaction suggested that versican cleavage by ADAMTS proteases, and the presence of cleaved versican was required for regression of the IDT.

Fibulin-1, a co-factor for ADAMTS5-mediated versican proteolysis, co-localizes with versican and influences IDT regression

Fibulin-1, a modular ECM protein interacting with the G3 domain of versican, was previously reported to be a co-factor for ADAMTS1 proteolysis of aggrecan (Lee et al., 2005). In addition, the *C.elegans fibulin* gene, which is most closely related to mammalian fibulin-1 (Barth et al., 1998), interacts genetically with the ADAMTS proteases, *Mig-17* and *Gon-1* during gonadal morphogenesis (Hesselson et al., 2004; Kubota et al., 2004). Versican and fibulin-1 localization was analyzed by immunofluorescence in E14.5 *wt* and *Adamts5−/−; bt/bt* hindlimbs. Fibulin-1 colocalized with versican in the perichondrium in both genotypes (Fig. 5A shows wild-type staining). ADAMTS5 is the most active versicanase among the three proteases and is most closely related to ADAMTS1. Since the highest penetrance of STS among single gene deletions was in *Adamts5−/−* mice, we used a cell-based assay to determine whether fibulin-1 influenced ADAMTS5 processing of versican. ADAMTS5 was expressed alone or was co-expressed with fibulin-1 isoforms with different C-terminal domains, fibulin-1C and -1D, followed by incubation of the conditioned medium from these cells with versican-rich medium from vascular smooth muscle cells. Co-transfection of ADAMTS5 with fibulin-1C or -1D led to a significant increase in versicanase activity, as indicated by increased levels of the 70 kDa versican cleavage fragment containing the DPEAAE neoepitope on western blots (Fig. 5 B,C). Fibulin-1 was not proteolytically modified by ADAMTS5.

Given this observed effect and colocalization of fibulin-1 with versican, we hypothesized that fibulin-1 enhanced ADAMTS activity during IDT regression, and assessed the penetrance and severity of STS in *bt/bt*; *Fbln1+/−* mice. *Fbln1−/−* mice have severe vascular and lung anomalies and die peri-natally (Cooley et al., 2008; Kostka et al., 2001), and thus *bt/bt*; *Fbln-1 −/−* mice were not generated. *bt/bt*; *Fbln-1+/−* mice developed STS with high penetrance, similar to *Adamts5−/−; bt/bt* mice (Fig. 5D, Supplemental Fig. S4). This finding strongly suggested that fibulin-1 acted as a co-factor for at least one ADAMTS in IDT regression. We conclude that in the absence of *Adamts20* (*bt/bt* genotype), *Fbln1* haploinsufficiency lowered the activity of ADAMTS5 similar to that resulting from deficiency of both *Adamts20* and *Adamts5* and possibly reduced the activity of (an)other ADAMTS protease(s) also.

Versican expression and proteolysis are spatially regulated during IDT regression

Versican is a widely distributed proteoglycan in embryonic ECM, and a substrate of *Adamts5* (Longpre et al., 2009), *Adamts9* (Somerville et al., 2003) and *Adamts20* (Silver, 2008). Since versican proteolysis was defined as a critical event in web regression, we determined *Vcan* expression and localization relative to ADAMTS5 and fibulin-1 in further detail using *in situ* hybridization and immunolocalization. During limb development, *Vcan* was strongly upregulated in the precartilaginous mesenchyme of prospective digit cartilages at E12.5, whereas after E13.5, *Vcan* mRNA was confined to the perichondrium of both forelimbs and hindlimbs and to the tips of the digits (Fig. 6A). At E12.5 and E13.5, some *Vcan* expression was also present in IDT (Fig. 6A). Thus, its expression overlapped with *Adamts5*, *Adamts9* and *Adamts20* during autopod morphogenesis and web regression and corresponded temporally with them. To precisely define their spatial relationships, we used immunofluorescense to detect versican, cleaved versican, fibulin-1 and ADAMTS5 in serial sections of E14 hindlimb autopods. Versican localized to the broadest tissue domain, extending from the edge of digit cartilage to the IDT, where substantially lower staining intensity than perichondrium was seen (Fig. 6B). Fibulin-1 overlapped with versican in the perichondrium, and ADAMTS5 was juxtaposed with the most peripheral region of versican and fibulin-1 staining. Intriguingly, cleaved versican (representing cleaved N-terminal fragments ending in Glu^{441}) was located primarily in the IDT (Fig. 6B). These data suggest that only the most peripherally located versican in the digit perichondrium is likely to be cleaved by ADAMTS5, and demonstrate that cleaved versican is localized with the cell population that is destined to undergo apoptosis.

Application of ectopic BMP4 rescues apoptosis in *Adamts5−/−; bt/bt* IDT without inducing versican cleavage

We tested whether IDT cells in *Adamts5−/−; bt/bt* hindlimbs were responsive to BMP induction of apoptosis by local application of exogenous BMP4. Recombinant active BMP4, TGF 2 or bovine serum albumin (BSA, negative control) in a microbead carrier was delivered to the IDT between digits 3 and 4 of the right hindlimbs of E13.75 *Adamts5−/−; bt/bt* autopods, since this interdigit space consistently presented the most severe syndactyly (Fig. 3C, Supplemental Fig. S2A,B). Local application of BMP4 but not BSA induced apoptosis in the IDT (Fig. 6C), yet did so in the absence of increased versican cleavage in the vicinity of the bead. Although mice lacking both TGF 2 and TGF 3 have STS (Dunker et al., 2002), a bead soaked in TGF 2 did not induce apoptosis in these autopods (data not shown). These data suggest that in the presence of sufficiently high BMP levels, apoptosis can be induced without concomitant versican processing. These data also suggest that ADAMTS proteases are not downstream effectors of BMPs during IDT apoptosis.

Application of cleaved versican induces apoptosis in *Adamts5−/−;bt/bt* webs

Since the genetic interactions described above, together with the presence of cleaved versican in the interdigital webs pointed to a potential mechanistic role for cleaved versican, we generated recombinant G1-DPEAAE[441] versican representing a product of ADAMTS activity (Fig. 7A). A bead soaked in conditioned medium from HEK293F cells stably expressing this fragment was inserted into the mutant webs as described above for BMP-4. Medium from cells transfected with an empty vector was used as the negative control. As shown in Fig. 7B, the versican fragment induced apoptosis in *Adamts5−/−; bt/bt* webs (n=6), whereas in the control experiments (n=6), apoptosis was primarily seen at the margins of the bead. These data suggested that the product of versican cleavage by ADAMTS proteases enabled interdigital apoptosis.

DISCUSSION

This work identifies a mechanism for ECM clearance during web regression and suggests that distinct *Adamts* gene products work cooperatively with each other and synchronously with pro-apoptotic mechanisms during web regression. The temporal and spatial overlap between ADAMTS proteases and versican, together with persistent uncleaved versican and decreased DPEAAE immunoreactivity in *Adamts5−/−; bt/bt* IDT, are strongly suggestive of an essential role for ADAMTS5, ADAMTS9, and ADAMTS20 in versican processing during IDT regression. The data not only suggest that ADAMTS proteolysis of versican during IDT resorption is facilitated by fibulin-1, but also that cleaved versican is required for web regression, possibly by sensitization of IDT cells to pro-apoptotic factors such as BMPs (Fig. 7C).

The observed effects of allele dosage suggest that the combined proteolytic activity of at least three ADAMTS proteases, ADAMTS5, ADAMTS9 and ADAMTS20 (and possibly ADAMTS1) normally maintains proteolysis of versican above a critical hypothetical threshold required for complete IDT regression (Fig. 7D). Removal of a single versican-degrading ADAMTS protease may reduce proteolytic activity to around the level of the threshold, in which case incompletely penetrant syndactyly is observed, as in *bt/bt* or *Adamts5−/−* mice (Fig. 7D). When two or more ADAMTS proteases are deleted (e.g. *Adamts5−/−; bt/bt* mice), proteolytic activity drops below the threshold and a higher penetrance of syndactyly is observed (Fig. 7D). Sub-threshold proteolysis also results from reduction of fibulin-1, a co-factor for ADAMTS5, and therefore has a similar outcome as reduction of *Adamts5* alleles in *bt* mice (Fig. 7D). Fibulin-1 may also act as a co-factor for other ADAMTS proteases. Alternately, *Fbln1* haploinsufficiency may affect the formation of versican-containing networks. A complex synpolydactyly has been reported as a result of rearrangement of *FBLN1* in humans (Debeer et al., 2002). However, limb defects have not been reported in *Fbln1−/−* mice.

The observed variation in severity of STS, and the fact that not all interdigital spaces are affected in compound ADAMTS-deficient mice strongly suggests that additional versican-degrading ADAMTS proteases are involved. We excluded a role for ADAMTS4 by genetic analysis and showed that *Adamts8* was not expressed in the autopod, but our studies most likely underestimated the contribution of ADAMTS9, since it cannot be completely deleted in IDT at the present time. *Adamts1* is highly expressed in the IDT during web regression (Thai and Iruela-Arispe, 2002) but combinatorial deletion of *Adamts1* and *Adamts5* is currently untenable since these genes are tightly linked (70 kb apart) on mouse chromosome 16 (Koo et al., 2007).

Taken together, the experimental observations comprising genetic interactions, overlapping mRNA expression and protein localization, and biochemical interactions, are consistent with the existence of a molecular network in ECM comprised of ADAMTS5, ADAMTS9, ADAMTS20, versican and fibulin-1, that influences apoptosis during IDT resorption. Binary biochemical interactions have been previously demonstrated between versican and fibulin-1, ADAMTS1 and fibulin-1, and ADAMTS proteases (specifically, ADAMTS1, ADAMTS4, ADAMTS5, ADAMTS9 and ADAMTS20) and versican (Aspberg et al., 1999; Lee et al., 2005; Longpre et al., 2009; Olin et al., 2001; Sandy et al., 2001; Silver, 2008; Somerville et al., 2003).

We investigated possible connections between this extracellular network and apoptosis *in vivo*. The data suggest that ADAMTS proteases are not upstream of either BMP or FGF signaling mechanisms, since the BMP-FGF axis and BMP signaling were unimpaired in the absence of ADAMTS5 and ADAMTS20. Induction of apoptosis by BMP4 without concurrent versican proteolysis in *Adamts5−/−; bt/bt* IDT suggested that: **1**. In the presence of a high local

concentration of BMP, versican proteolysis was not required, and, **2**. Neither ADAMTS5 nor ADAMTS20 normally acted immediately downstream of BMP4. Normal BMP and FGF expression and BMP signaling in *Adamts5−/−; bt/bt* autopods argues against a role for ADAMTS proteases in release of BMPs or FGFs sequestered in ECM. It has been established that BMPs induce apoptosis when the local environment is permissive (Ganan et al., 1996; Guha et al., 2002; Merino et al., 1999b; Zou and Niswander, 1996) and we considered whether ADAMTS proteolysis of versican contributed to the permissiveness of the cellular environment at the critical developmental stage when IDT regression occurs.

Initially, we asked whether versican was simply a passive target of the ADAMTS proteases to be cleared concurrently with cells as part of normal IDT regression. However, since *hdf/+* mice do not have STS, and because STS in *bt/bt; hdf/+* mice is as penetrant as in *bt/bt; Adamts5−/−* mice, we propose that cleaved rather than intact versican is necessary for web regression. The observation of cleaved versican within the IDT at a site remote from the highest concentrations of intact versican raises the intriguing possibility that versican fragments may move into the IDT where they may bind to cells or disrupt cell-matrix interactions. The traditional developmental roles of versican as an anti-adhesive molecule, a barrier for cell migration, or in defining migratory pathways of neural crest cells (Dutt et al., 2006; Perissinotto et al., 2000) implied passive mechanisms. However, recent work has demonstrated intriguing effects of versican and recombinant versican domains on cell proliferation, senescence and apoptosis, although these are poorly understood (LaPierre et al., 2007; Suwan et al., 2009). Since the requirement for versican processing is bypassed by insertion of a BMP4 soaked bead, we speculated that versican fragments may lower the threshold of BMP required to induce apoptosis. Indeed, the versican G1-DPEAAE^{441} fragment, expressed as a recombinant protein, could induce apoptosis in the mutant web. We propose that proteolysis of versican is permissive for BMP-induced apoptosis during normal development, i.e., concurrent versican processing and BMP upregulation enable interdigit cell apoptosis (Fig. 7C).

The evolution of mammalian limb development to require multiple proteases for web regression is, upon initial contemplation, quite surprising, since nature is parsimonious. However, *Adamts5, Adamts1*, *Adamts9* and *Adamts20* mRNAs are also expressed in an overlapping fashion at other sites during development (Jungers et al., 2005; McCulloch et al., 2009; Thai and Iruela-Arispe, 2002). Versican, fibulins, and these versican-degrading ADAMTS proteases are all present in the developing cardiac outflow tract, during craniofacial development, and in the arterial wall, myocardium, skin and central nervous system (Bode-Lesniewska et al., 1996; Kern et al., 2007; Stankunas et al., 2008; Zhang et al., 1995; Zhang et al., 1996). Recent work implicated versican processing by ADAMTS1 in remodeling of the embryonic myocardium and cardiac outflow tract (Kern et al., 2007; Stankunas et al., 2008) and during ovulation (Russell et al., 2003). It is possible, although as yet unconfirmed, that the molecular network identified here, as well as bioactive versican fragments, may participate in other developmental processes as well.

ADAMTS5 is a key pathogenic protease and drug target in arthritis, since *Adamts5−/−* mice do not develop arthritis following induction of inflammation or mechanical instability in their knees (Glasson et al., 2005; Stanton et al., 2005). ADAMTS5 was previously thought not to have a developmental role. The proposed threshold model of ADAMTS proteolysis (Fig. 7A) suggests that the detection of *Adamts* phenotypes may be masked in mice lacking a single ADAMTS protease, or that the severity of observed phenotypes may be underestimated. Combinatorial transgenes for proteoglycan-degrading ADAMTS proteases are therefore likely to be insightful and relevant to several morphogenetic processes.

EXPERIMENTAL PROCEDURES

Additional methods and/or details are provided in the supplemental text.

Analysis of Transgenic Mice

Mouse strains, embryo preparation and β-gal histochemistry—All animal procedures were done at the Cleveland Clinic under an Institutional Animal Care and Use Committee approved protocol. Mice with targeted inactivation of *Adamts5* (*6.129P2-Adamts5tm1Dgen/J*, referred to as *Adamts5−/−*)(McCulloch et al., 2009)*, Adamts4*, and *Adamts9,* were generated by Deltagen (San Mateo, CA) and purchased from Jackson Laboratories (Bar Harbor, ME, *Adamts4* and *Adamts5*) or Deltagen (*Adamts9*). A mutant *Adamts20* allele, *belted, (Adamts20bt-Bei1* referred to as *bt)* (Rao et al., 2003) a *Vcan* mutant allele (*heart defect, hdf)* (Mjaatvedt et al., 1998) and *Fbln1* deficient mice (Cooley et al., 2008) were previously described. All observations were made in alleles that were backcrossed extensively to C57Bl/6 (*Adamts5*, 8 generations; *Adamts9* and *bt*, 10 generations each; *Fbln1,* 7 generations; *hdf*, 10 generations). These genes are expected to segregate independently, so combinatorial transgenic mice were generated by interbreeding. STS was scored as described in the Supplemental Methods.

Micro-computerized tomography (mCT) analysis: The following genotypes (no. of mice) were examined. *Adamts5−/−*, *bt/bt* mice (16); *Adamts5+/+*, *+/bt* (1); *Adamts5+/+*, *bt/bt* (1); *Adamts5+/−*, *+/bt* (1) and *Adamts5−/−*, *+/bt* (2), *Adamts5+/−* (1), wild-type (1). Mouse limbs werefixed in 70 % ethanol and scanned on an eXplore Locus SP instrument (General Electric). The scans were done at 80 kV peak and 500 μA with an exposure time of 3000 milliseconds. Three hundred and sixty views were done in a 1° increment over 360°. Scans were reconstructed using GE reconstruction software yielding a post-reconstruction resolution of 26 microns. Scans were visualized using GE Health Care Micro-View version ABA 2.1.2.

β-gal histochemistry, *In Situ* Hybridization (ISH), IHC and RT-PCR

Timed gestations, tissue fixation and β-gal histochemistry are described in the Supplemental Methods. Digoxigenin labeled cRNA probes were generated using reagents from Roche. Embryos obtained from timed gestations were processed for ISH as described in Supplemental Methods. Antibodies and methods used for IHC, RT-PCR primers and reaction conditions are described in Supplemental Methods.

Detection of apoptosis using acridine orange staining and TUNEL assays

E14.5 embryo limbs were incubated in PBS for 30 min at room temperature and in 0.1 μg/ml acridine orange (AO) (Sigma-Aldrich) in PBS for 10 min. Limbs were washed twice in PBS and viewed under an inverted fluorescent microscope (Leica) within 2 h of staining. *Adamts5 −/−; bt/bt* and *Adamts5−/−; bt/+* littermates (controls) were stained with AO. Apoptosis was scored by one of the authors (LJD) blinded to the genotype. Detection of apoptotic cells by the TUNEL method was done using a kit (Promega Corp, Madison, WI).

Ex Vivo Limb Culture and bead application

Affigel beads (Bio-Rad, Hercules, CA) were soaked in 100 μg/ml recombinant BMP-4 (R&D systems, Minneapolis, MN), 50 μg/ml recombinant TGFβ, 100 μg/ml Bovine Serum Albumin (BSA) (Sigma-Aldrich), conditioned medium of G1-DPEAAE[441] expressing HEK293F cells or the control medium for 1 h at room temperature. E13.75 *Adamts5−/−; bt/bt* hindlimb autopods were dissected and placed in culture medium optimized for these cultures (1:1 DMEM:Ham's F12 plus 0.1 % FBS). Size-matched presoaked Affigel beads were inserted in the web space between digits 3 and 4. Autopods were placed on a Nuclepore 8 μm pore-size

filter (Whatman, Florham Park, NJ) in a 24-well tissue culture dish, and cultured at the air-liquid interface. Hindlimbs were incubated for 14 h at 37 °C in 5 % CO_2 followed by AO staining or TUNEL assay on paraffin sections. For bead insertion of G1-DPEAAE[441], Nuclepore 0.1um pore size track-etch membrane was used.

Cell culture, transfections, versicanase assay and western blotting

HEK293F cells (ATCC, Manassus, VA) were cultured in Dulbecco's Modified Eagles Medium (DMEM) supplemented with 10 % FBS and antibiotics. Expression plasmids for Myc-tagged *Adamts5*, fibulin-1C and -1D, and Gremlin, were transiently co-transfected into HEK293F cells using FUGENE-6 (Roche Diagnostics, Indianapolis, IN). In the case of control *Adamts5* co-transfection, empty vector (pcDNA3.1 MychHis, Invitrogen) was co-transfected with the *Adamts5* construct. Serum-free media and cell lysates were collected after 24 h. Cells were lysed in 1% Triton X-100, 10 mM Tris.HCl, pH 7.6 containing complete protease inhibitor cocktail (Roche Diagnostics, Indianapolis, IN). Conditioned medium was combined with versican-rich medium obtained from cultured human vascular smooth muscle cells at a 1:1 ratio, and incubated for 12h to 18 h at 37°C, followed by treatment with protease-free chondroitinase ABC (Seikagaku, Tokyo, Japan) for 2 h at 37°C. Western blotting was done under reducing conditions using anti-DPEAAE (Affinity Bioreagents, Golden, CO), anti-fibulin-1 (Sasaki et al., 1995), or anti-myc monoclonal antibody 9E10 (Invitrogen, Carlsbad, CA) and enhanced chemiluminescence (ECL, GE Healthcare, Piscataway, NJ). Band intensity was quantitated using IMAGE J software (NIH, Bethesda, MD). A type 1 (paired), 2-tailed student's t-test was used to determine whether the normalized data obtained from the ImageJ software was statistically significant.

Supplementary Material

Refer to Web version on PubMed Central for supplementary material.

Acknowledgments

REFERENCES

Apte SS. A disintegrin-like and metalloprotease (reprolysin-type) with thrombospondin type 1 motif (ADAMTS) superfamily-functions and mechanisms. J Biol Chem. 2009

Arner EC, Pratta MA, Trzaskos JM, Decicco CP, Tortorella MD. Generation and characterization of aggrecanase. A soluble, cartilage-derived aggrecan-degrading activity. J Biol Chem 1999;274:6594–6601. [PubMed: 10037754]

Aspberg A, Adam S, Kostka G, Timpl R, Heinegard D. Fibulin-1 is a ligand for the C-type lectin domains of aggrecan and versican. J Biol Chem 1999;274:20444–20449. [PubMed: 10400671]

Bandyopadhyay A, Tsuji K, Cox K, Harfe BD, Rosen V, Tabin CJ. Genetic analysis of the roles of BMP2, BMP4, and BMP7 in limb patterning and skeletogenesis. PLoS Genet 2006;2:e216. [PubMed: 17194222]

Barth JL, Argraves KM, Roark EF, Little CD, Argraves WS. Identification of chicken and C. elegans fibulin-1 homologs and characterization of the C. elegans fibulin-1 gene. Matrix Biol 1998;17:635–646. [PubMed: 9923656]

Bode-Lesniewska B, Dours-Zimmermann MT, Odermatt BF, Briner J, Heitz PU, Zimmermann DR. Distribution of the large aggregating proteoglycan versican in adult human tissues. J Histochem Cytochem 1996;44:303–312. [PubMed: 8601689]

Boulet AM, Moon AM, Arenkiel BR, Capecchi MR. The roles of Fgf4 and Fgf8 in limb bud initiation and outgrowth. Dev Biol 2004;273:361–372. [PubMed: 15328019]

Cooley MA, Kern CB, Fresco VM, Wessels A, Thompson RP, McQuinn TC, Twal WO, Mjaatvedt CH, Drake CJ, Argraves WS. Fibulin-1 is required for morphogenesis of neural crest-derived structures. Dev Biol 2008;319:336–345. [PubMed: 18538758]

Dahn RD, Fallon JF. Interdigital regulation of digit identity and homeotic transformation by modulated BMP signaling. Science 2000;289:438–441. [PubMed: 10903202]

Debeer P, Schoenmakers EF, Twal WO, Argraves WS, De Smet L, Fryns JP, Van De Ven WJ. The fibulin-1 gene (FBLN1) is disrupted in a t(12;22) associated with a complex type of synpolydactyly. J Med Genet 2002;39:98–104. [PubMed: 11836357]

Dunker N, Schmitt K, Krieglstein K. TGF-beta is required for programmed cell death in interdigital webs of the developing mouse limb. Mech Dev 2002;113:111–120. [PubMed: 11960699]

Dutt S, Kleber M, Matasci M, Sommer L, Zimmermann DR. Versican V0 and V1 guide migratory neural crest cells. J Biol Chem 2006;281:12123–12131. [PubMed: 16510447]

Ganan Y, Macias D, Duterque-Coquillaud M, Ros MA, Hurle JM. Role of TGF beta s and BMPs as signals controlling the position of the digits and the areas of interdigital cell death in the developing chick limb autopod. Development 1996;122:2349–2357. [PubMed: 8756280]

Glasson SS, Askew R, Sheppard B, Carito B, Blanchet T, Ma HL, Flannery CR, Peluso D, Kanki K, Yang Z, et al. Deletion of active ADAMTS5 prevents cartilage degradation in a murine model of osteoarthritis. Nature 2005;434:644–648. [PubMed: 15800624]

Gross J, Lapiere CM. Collagenolytic activity in amphibian tissues: a tissue culture assay. Proc Natl Acad Sci U S A 1962;48:1014–1022. [PubMed: 13902219]

Guha U, Gomes WA, Kobayashi T, Pestell RG, Kessler JA. In vivo evidence that BMP signaling is necessary for apoptosis in the mouse limb. Dev Biol 2002;249:108–120. [PubMed: 12217322]

Hesselson D, Newman C, Kim KW, Kimble J. GON-1 and fibulin have antagonistic roles in control of organ shape. Curr Biol 2004;14:2005–2010. [PubMed: 15556862]

Jungers KA, Le Goff C, Somerville RP, Apte SS. Adamts9 is widely expressed during mouse embryo development. Gene Expr Patterns 2005;5:609–617. [PubMed: 15939373]

Kern CB, Norris RA, Thompson RP, Argraves WS, Fairey SE, Reyes L, Hoffman S, Markwald RR, Mjaatvedt CH. Versican proteolysis mediates myocardial regression during outflow tract development. Dev Dyn 2007;236:671–683. [PubMed: 17226818]

Kimata K, Oike Y, Tani K, Shinomura T, Yamagata M, Uritani M, Suzuki S. A large chondroitin sulfate proteoglycan (PG-M) synthesized before chondrogenesis in the limb bud of chick embryo. J Biol Chem 1986;261:13517–13525. [PubMed: 3759975]

Koo BH, Goff CL, Jungers KA, Vasanji A, O'Flaherty J, Weyman CM, Apte SS. ADAMTS-like 2 (ADAMTSL2) is a secreted glycoprotein that is widely expressed during mouse embryogenesis and is regulated during skeletal myogenesis. Matrix Biol. 2007

Kostka G, Giltay R, Bloch W, Addicks K, Timpl R, Fassler R, Chu ML. Perinatal lethality and endothelial cell abnormalities in several vessel compartments of fibulin-1-deficient mice. Mol Cell Biol 2001;21:7025–7034. [PubMed: 11564885]

Kubota Y, Kuroki R, Nishiwaki K. A fibulin-1 homolog interacts with an ADAM protease that controls cell migration in C. elegans. Curr Biol 2004;14:2011–2018. [PubMed: 15556863]

LaPierre DP, Lee DY, Li SZ, Xie YZ, Zhong L, Sheng W, Deng Z, Yang BB. The ability of versican to simultaneously cause apoptotic resistance and sensitivity. Cancer Res 2007;67:4742–4750. [PubMed: 17510402]

Lee NV, Rodriguez-Manzaneque JC, Thai SN, Twal WO, Luque A, Lyons KM, Argraves WS, Iruela-Arispe ML. Fibulin-1 acts as a cofactor for the matrix metalloprotease ADAMTS-1. J Biol Chem. 2005

Llamazares M, Cal S, Quesada V, Lopez-Otin C. Identification and characterization of ADAMTS-20 defines a novel subfamily of metalloproteinases-disintegrins with multiple thrombospondin-1 repeats and a unique GON domain. J Biol Chem 2003;278:13382–13389. [PubMed: 12562771]

Longpre JM, McCulloch DR, Koo BH, Alexander JP, Apte SS, Leduc R. Characterization of proADAMTS5 processing by proprotein convertases. Int J Biochem Cell Biol 2009;41:1116–1126. [PubMed: 18992360]

Lu P, Minowada G, Martin GR. Increasing Fgf4 expression in the mouse limb bud causes polysyndactyly and rescues the skeletal defects that result from loss of Fgf8 function. Development 2006;133:33–42. [PubMed: 16308330]

Matsumoto K, Shionyu M, Go M, Shimizu K, Shinomura T, Kimata K, Watanabe H. Distinct interaction of versican/PG-M with hyaluronan and link protein. J Biol Chem 2003;278:41205–41212. [PubMed: 12888576]

McCulloch DR, Goff CL, Bhatt S, Dixon LJ, Sandy JD, Apte SS. Adamts5, the gene encoding a proteoglycan-degrading metalloprotease, is expressed by specific cell lineages during mouse embryonic development and in adult tissues. Gene Expr Patterns 2009;9:314–323. [PubMed: 19250981]

Merino R, Ganan Y, Macias D, Rodriguez-Leon J, Hurle JM. Bone morphogenetic proteins regulate interdigital cell death in the avian embryo. Ann N Y Acad Sci 1999a;887:120–132. [PubMed: 10668469]

Merino R, Rodriguez-Leon J, Macias D, Ganan Y, Economides AN, Hurle JM. The BMP antagonist Gremlin regulates outgrowth, chondrogenesis and programmed cell death in the developing limb. Development 1999b;126:5515–5522. [PubMed: 10556075]

Mjaatvedt CH, Yamamura H, Capehart AA, Turner D, Markwald RR. The Cspg2 gene, disrupted in the hdf mutant, is required for right cardiac chamber and endocardial cushion formation. Dev Biol 1998;202:56–66. [PubMed: 9758703]

Olin AI, Morgelin M, Sasaki T, Timpl R, Heinegard D, Aspberg A. The proteoglycans aggrecan and Versican form networks with fibulin-2 through their lectin domain binding. J Biol Chem 2001;276:1253–1261. [PubMed: 11038354]

Pajni-Underwood S, Wilson CP, Elder C, Mishina Y, Lewandoski M. BMP signals control limb bud interdigital programmed cell death by regulating FGF signaling. Development 2007;134:2359–2368. [PubMed: 17537800]

Perissinotto D, Iacopetti P, Bellina I, Doliana R, Colombatti A, Pettway Z, Bronner-Fraser M, Shinomura T, Kimata K, Morgelin M, et al. Avian neural crest cell migration is diversely regulated by the two major hyaluronan-binding proteoglycans PG-M/versican and aggrecan. Development 2000;127:2823–2842. [PubMed: 10851128]

Rao C, Foernzler D, Loftus SK, Liu S, McPherson JD, Jungers KA, Apte SS, Pavan WJ, Beier DR. A defect in a novel ADAMTS family member is the cause of the belted white-spotting mutation. Development 2003;130:4665–4672. [PubMed: 12925592]

Russell DL, Doyle KM, Ochsner SA, Sandy JD, Richards JS. Processing and localization of ADAMTS-1 and proteolytic cleavage of versican during cumulus matrix expansion and ovulation. J Biol Chem 2003;278:42330–42339. [PubMed: 12907688]

Salas-Vidal E, Valencia C, Covarrubias L. Differential tissue growth and patterns of cell death in mouse limb autopod morphogenesis. Dev Dyn 2001;220:295–306. [PubMed: 11307164]

Sandy JD, Westling J, Kenagy RD, Iruela-Arispe ML, Verscharen C, Rodriguez-Mazaneque JC, Zimmermann DR, Lemire JM, Fischer JW, Wight TN, et al. Versican V1 proteolysis in human aorta in vivo occurs at the Glu441- Ala442 bond, a site that is cleaved by recombinant ADAMTS-1 and ADAMTS- 4. J Biol Chem 2001;276:13372–13378. [PubMed: 11278559]

Sasaki T, Kostka G, Gohring W, Wiedemann H, Mann K, Chu ML, Timpl R. Structural characterization of two variants of fibulin-1 that differ in nidogen affinity. J Mol Biol 1995;245:241–250. [PubMed: 7844816]

Silver DL, Hou L, Somerville R, Young ME, Apte SS, Pavan WJ. The secreted metalloprotease ADAMTS20 is required for melanoblast survival. PLoS Genet 2008;4:1–15.

Somerville RP, Longpre JM, Jungers KA, Engle JM, Ross M, Evanko S, Wight TN, Leduc R, Apte SS. Characterization of ADAMTS-9 and ADAMTS-20 as a distinct ADAMTS subfamily related to Caenorhabditis elegans GON-1. J Biol Chem 2003;278:9503–9513. [PubMed: 12514189]

Stankunas K, Hang CT, Tsun ZY, Chen H, Lee NV, Wu JI, Shang C, Bayle JH, Shou W, Iruela-Arispe ML, et al. Endocardial Brg1 represses ADAMTS1 to maintain the microenvironment for myocardial morphogenesis. Dev Cell 2008;14:298–311. [PubMed: 18267097]

Stanton H, Rogerson FM, East CJ, Golub SB, Lawlor KE, Meeker CT, Little CB, Last K, Farmer PJ, Campbell IK, et al. ADAMTS5 is the major aggrecanase in mouse cartilage in vivo and in vitro. Nature 2005;434:648–652. [PubMed: 15800625]

Suwan K, Choocheep K, Hatano S, Kongtawelert P, Kimata K, Watanabe H. Versican/PG-M assembles hyaluronan into extracellular matrix and inhibits CD44-mediated signaling toward premature senescence in embryonic fibroblasts. J Biol Chem. 2009

Thai SN, Iruela-Arispe ML. Expression of ADAMTS1 during murine development. Mech Dev 2002;115:181–185. [PubMed: 12049787]

Weatherbee SD, Behringer RR, Rasweiler J.J.t. Niswander LA. Interdigital webbing retention in bat wings illustrates genetic changes underlying amniote limb diversification. Proc Natl Acad Sci U S A 2006;103:15103–15107. [PubMed: 17015842]

Zhang HY, Chu ML, Pan TC, Sasaki T, Timpl R, Ekblom P. Extracellular matrix protein fibulin-2 is expressed in the embryonic endocardial cushion tissue and is a prominent component of valves in adult heart. Dev Biol 1995;167:18–26. [PubMed: 7851641]

Zhang HY, Timpl R, Sasaki T, Chu ML, Ekblom P. Fibulin-1 and fibulin-2 expression during organogenesis in the developing mouse embryo. Dev Dyn 1996;205:348–364. [PubMed: 8850569]

Zou H, Niswander L. Requirement for BMP signaling in interdigital apoptosis and scale formation. Science 1996;272:738–741. [PubMed: 8614838]

Zuzarte-Luis V, Hurle JM. Programmed cell death in the developing limb. Int J Dev Biol 2002;46:871–876. [PubMed: 12455623]
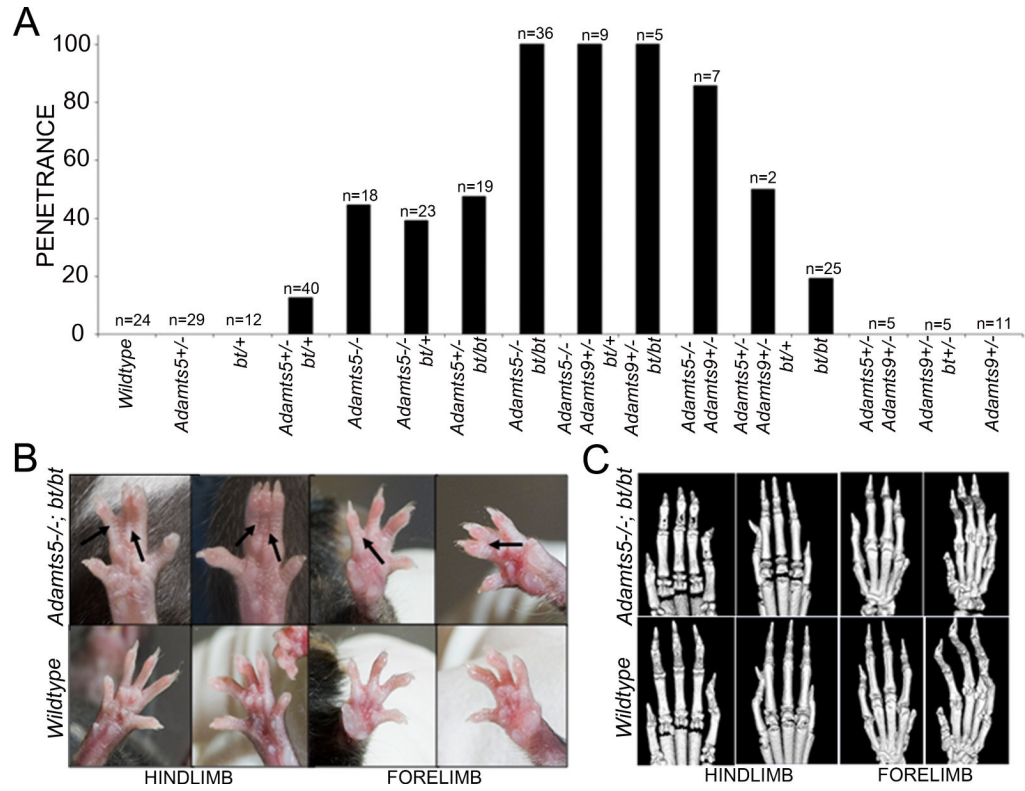
Figure 1. Combinatorial mutant *Adamts* alleles develop STS with greater penetrance than single *Adamts* mutants
A. Histogram of penetrance of STS in mice of the indicated genotype. The number of mice evaluated for each genotype is indicated above each bar. Note the general trend towards a higher penetrance with increasing dosage of inactivated (*Adamts5, Adamts9*) or mutant (*bt*) alleles. **B**. Representative types of STS seen in *Adamts5−/−; bt/bt* forelimbs and hindlimbs compared to wild-type limbs. Arrows indicate persistent interdigital webs. **C**. Three-dimensional reconstruction following mCT analysis of 3 week-old *Adamts5−/−; bt/bt* paws shows normal patterning and no radiological anomalies. Wild-type limbs are shown as controls.
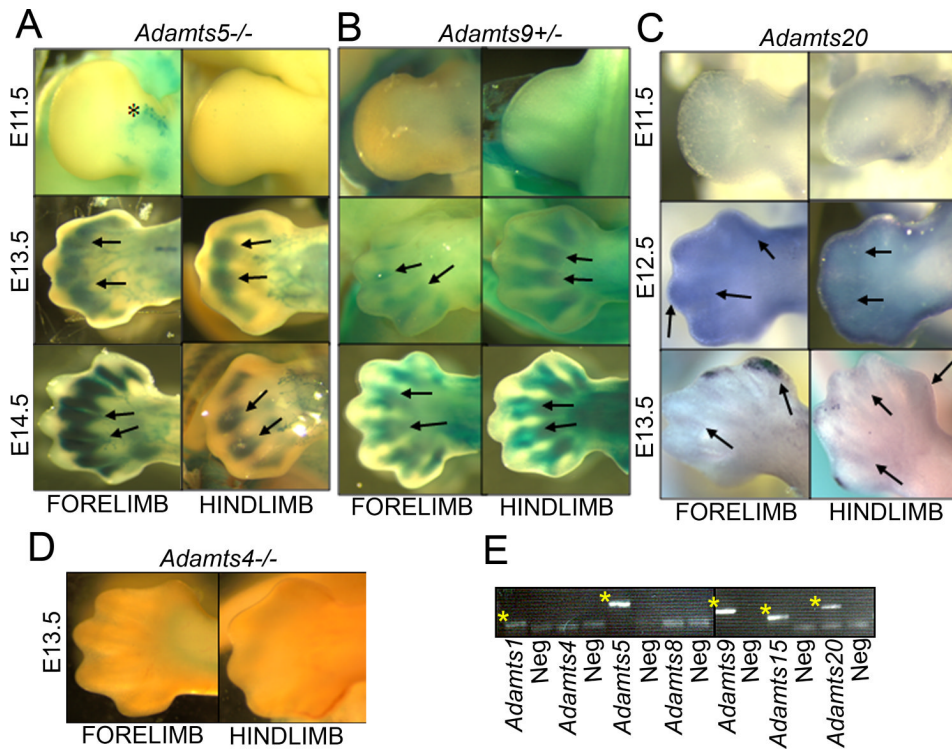
**Figure 2. Expression of *Adamts* genes in the developing autopod**
A and B. β-gal staining (blue-green) was used to profile *Adamts5* (**A**) and *Adamts9* (**B**) expression in forelimb and hindlimb autopods from E11.5 through E14.5. Note strong interdigital staining at E13.5 and E14.5 (arrows). The asterisk in the E11.5 *Adamts5−/−* autopod indicates staining of the brachial plexus. **C.** *In situ* hybridization of *Adamts20* in E11.5, E12.5, and E13.5 autopods. Diffuse expression was seen in the IDT at E12.5 and E13.5, and in the medial and lateral edges of the autopod (arrows). **D**. β-gal staining of *Adamts4−/−* autopods shows weak expression in forelimb IDT at E13.5. **E**. RT-PCR of RNA extracted from E13.5 wild-type hindlimbs. Specific amplicons are indicated by yellow asterisks. Neg: control PCR using water in place of cDNA.
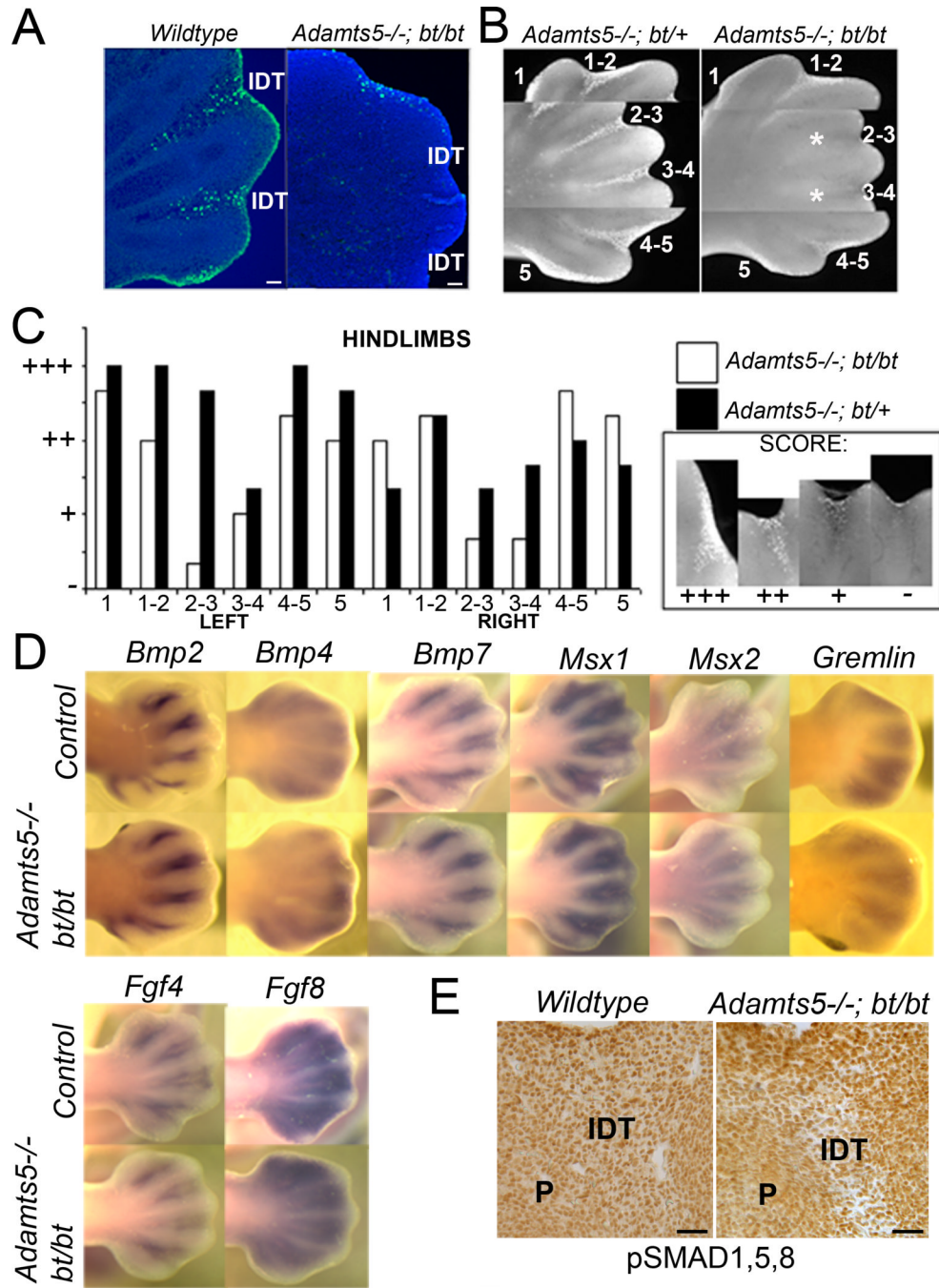
Figure 3. *Adamts5−/−; bt/bt* **autopods have decreased apoptosis but a normal BMP-FGF axis**
A. TUNEL staining of a section from wild-type E14.5 hindlimb autopod (control) shows the expected distribution of apoptoptic cells in the IDT (green fluorescence); TUNEL positive cells are absent in the IDT between digits 2 and 3 as well as between digits 3 and 4 of *Adamts5−/−;bt/bt* mice. The image is representative of 3 separately stained hindlimbs. Nuclei are stained blue using DAPI. Scale bar equals 50 μM. **B.** Acridine orange staining of E14.5 hindlimbs showing staining in the IDT of *Adamts5−/−; bt/+* mice, whereas staining is absent in the indicated *Adamts5−/−; bt/bt* IDT (white asterisks). Similar results were obtained in forelimbs of *Adamts5−/−; bt/bt* mice at E13.5. **C.** Acridine orange staining was scored in each hindlimb interdigital space in a blinded fashion according to the scoring scheme shown on the right. In

Adamts5−/−; bt/bt hindlimbs (n=6), the IDT between hindlimb digits 2 and 3 and digits 3 and 4 consistently had fewer stained cells than the control genotype (*Adamts5−/−*, *bt/+*) hindlimbs (n=6). **D.** Hindlimb autopods stained by whole mount *in situ* hybridization with the indicated probes shows comparable mRNA expression in E13.5 *Adamts5−/−; bt/bt* mice and controls. Similar expression was obtained in forelimbs. **E**. pSmad 1/5/8 immunohistochemistry demonstrates nuclear pSmad staining in both mutant and wild-type E14.5 hindlimb webs. Scale bar equals 50 μM.
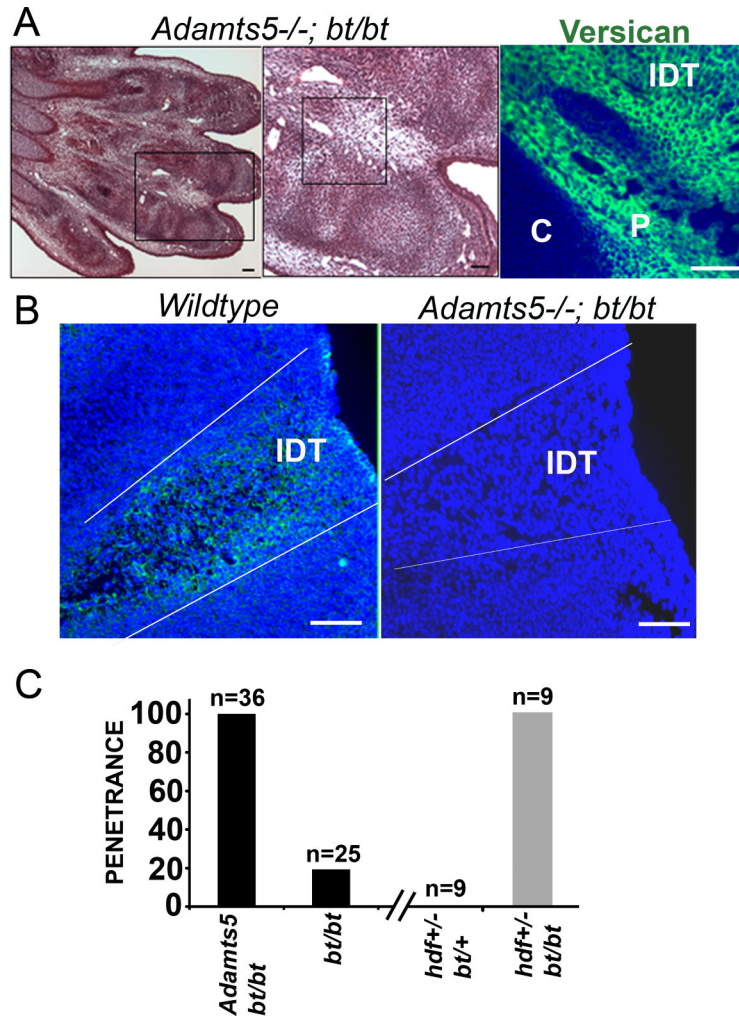
**Figure 4. Reduced versican processing in *Adamts5−/−; bt/bt* IDT, and increased STS in *bt/bt; Vcan +/−* mice**
A. An E16.5 hindlimb from an *Adamts5−/−; bt/bt* mouse shows lack of IDT resorption between digits 3 and 4 (boxed area, left-hand panel). The boxed area is enlarged in the center panel to illustrate a low cell density and loose ECM in the unresorbed IDT, suggestive of proteoglycan accumulation. The non-regressed ECM stains strongly with an anti-versican GAG antibody (right-hand panel, green signal). Scale bar equals 50 μm. **B.** Cleaved versican identified by anti-DPEAAE staining (green) is present in the IDT of an E14.5 wild-type hindlimb (left-hand panel). In contrast, greatly reduced anti-DPEAAE staining is seen in E14.5 *Adamts5−/−; bt/ bt* hindlimb IDT (right-hand panel). Scale bar equals 50 μm. **C.** STS in *bt/bt; hdf/+* mice. Data indicating penetrance in *Adamts5−/−; bt/bt* mice, and *bt/bt* mice (black bars), are taken from Fig. 1. Note the lack of syndactyly in compound heterozygotes of *bt* and *hdf* and the greatly increased penetrance in *bt/bt; hdf+* mice (gray bar).
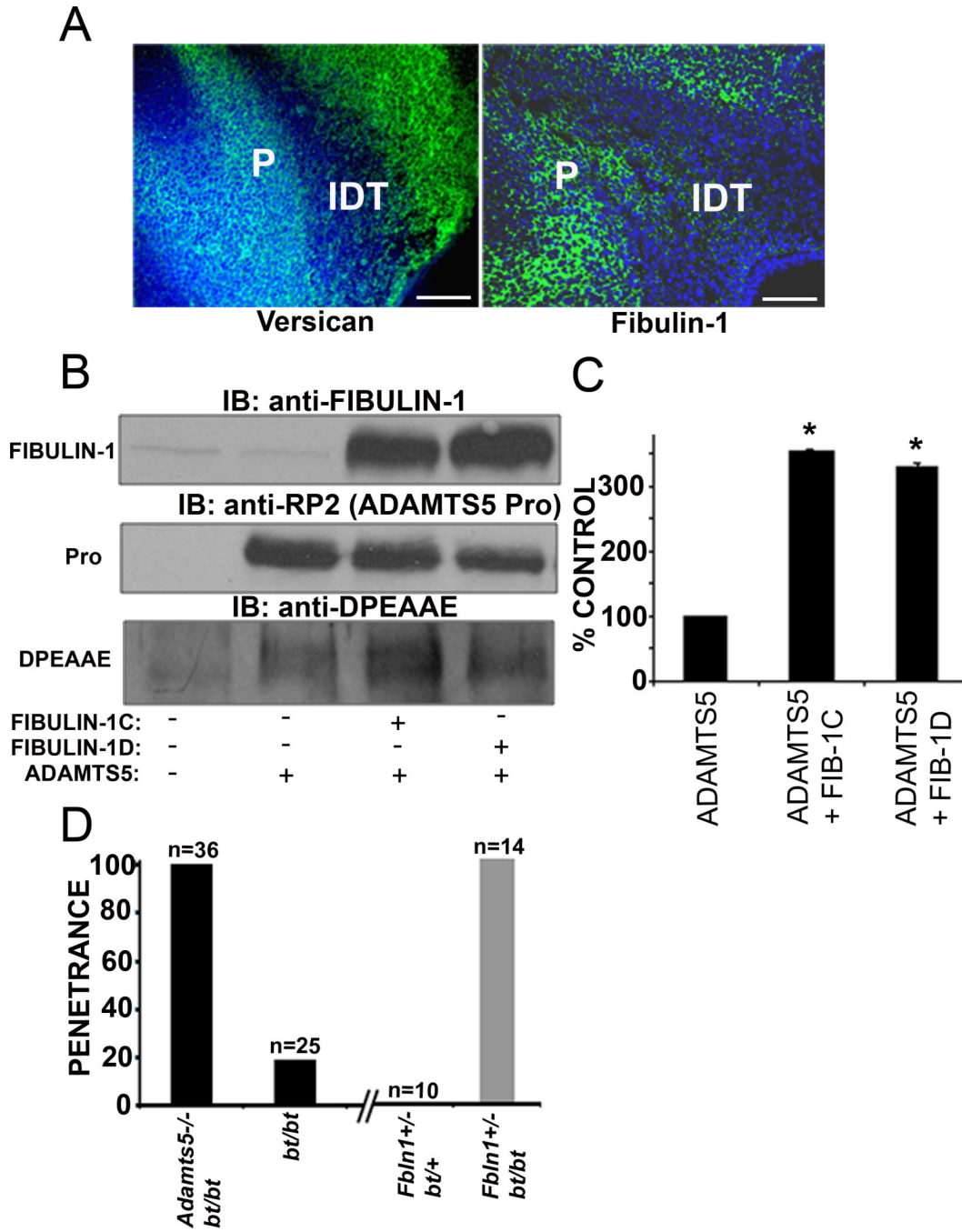
Figure 5. Fibulin-1 and versican co-localize in the IDT and fibulin-1 acts as a co-factor for *Adamts5*-mediated versican proteolysis
**A.** Intact versican (GAGß, green, left-hand panel) has a similar localization as fibulin-1 (green, right-hand panel) in E14.5 wild-type hindlimb perichondrium (P). A weak signal is present in IDT. These data are representative of 3 stained autopods. Nuclei are stained blue by DAPI. Scale bar equals 50 μM. **B.** Fibulin-1 enhances ADAMTS5 processing of versican. Western blots show expression of fibulin-1C, and fibulin-1D (upper panel) in cell lysates from HEK293F cells co-transfected with full-length *Adamts5* (detected by a propeptide specific antibody RP-2, center panel). Anti-DPEAAE was used to detect the cleaved 70 kDa versican species in the medium (lower panel). **C.** Quantification of anti-DPEAAE reactive molecular

species in medium of cells expressing ADAMTS5 alone, or ADAMTS5 plus fibulin-1C or fibulin 1-D. Levels of anti-DPEAAE-reactive peptide obtained by densitometry were normalized to levels of *Adamts5* propeptide and are representative of four independent experiments (data show mean ± S.E.M.). There is a statistically significant enhancement of versican processing by ADAMTS5 in the presence of both fibulin-1 isoforms (Student t-test, *p <0.05). **D**. Penetrance of syndactyly is increased in *bt/bt; Fbln1/+* mice compared to *bt/bt* and *Fbln1+/−; bt/+* mice, suggesting a genetic interaction between *Adamts5* and *Fbln1* (Note: *Fbln1* haploinsufficiency leads to STS in mice lacking ADAMTS20, thus uncovering a functional association with another ADAMTS protease, most likely ADAMTS5, as evidence by findings in panel B). Data for penetrance in *Adamts5−/−; bt/bt* mice and *bt/bt* mice (black bars) are taken from Fig. 1.
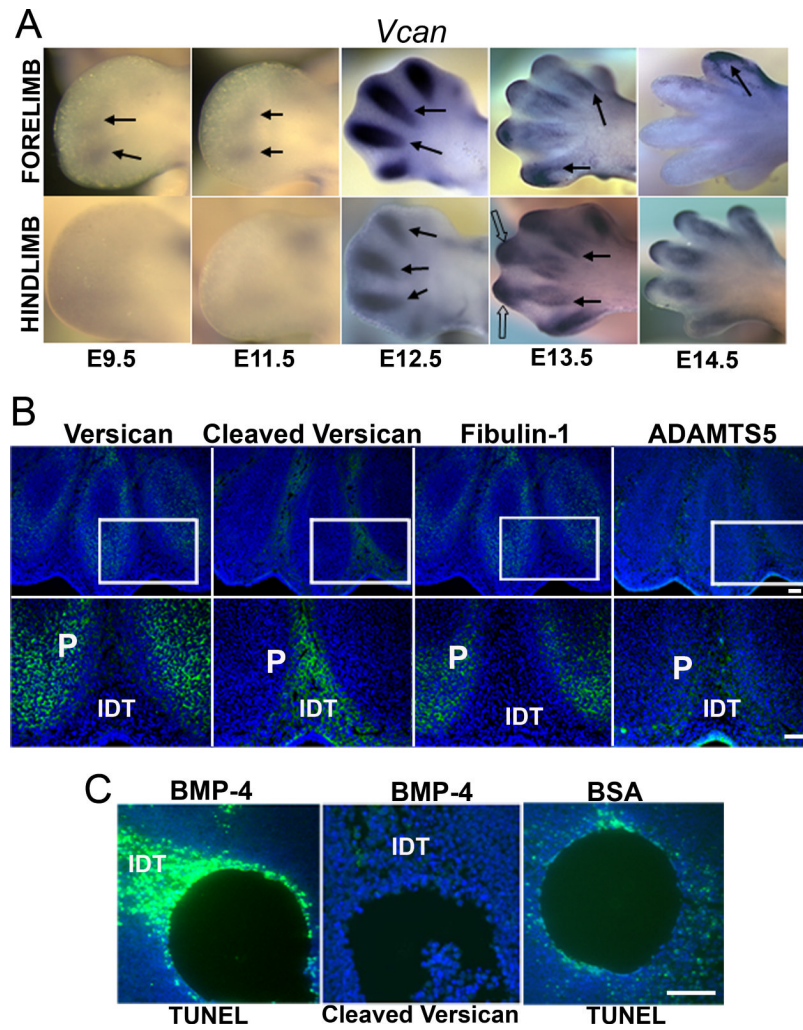
Figure 6. Versican expression and localization during autopod development and the effect of local BMP4 application on apoptosis and versican proteolysis
A. Whole-mount ISH with a *Vcan* probe shows strong expression in the precartilaginous mesenchyme of digital rays at E12.5 (arrows), with forelimb expression anticipating the hindlimb. At later stages, *Vcan* is strongly expressed in perichondrium (arrows at E13.5), with weak expression in the IDT. **B**. Serial sections from a wild-type E14.0 hindlimb autopod were immunostained with indicated antibodies to show the precise relationship between versican, cleaved versican, fibulin-1 and ADAMTS5. The boxed regions in the upper panels are enlarged in the lower panels. Cleaved versican is located in the IDT whereas the strongest signals for intact versican and fibulin-1 are present in the perichondrium (P). ADAMTS5 is located at the boundary between perichondrium and IDT. **C**. Implantation of a BMP4-soaked bead in E13.75 *Adamts5−/−; bt/bt* hindlimb IDT leads to apoptosis (TUNEL) but not to versican cleavage, whereas a bead soaked in BSA did not induce cell death. The result is representative of three independent experiments.
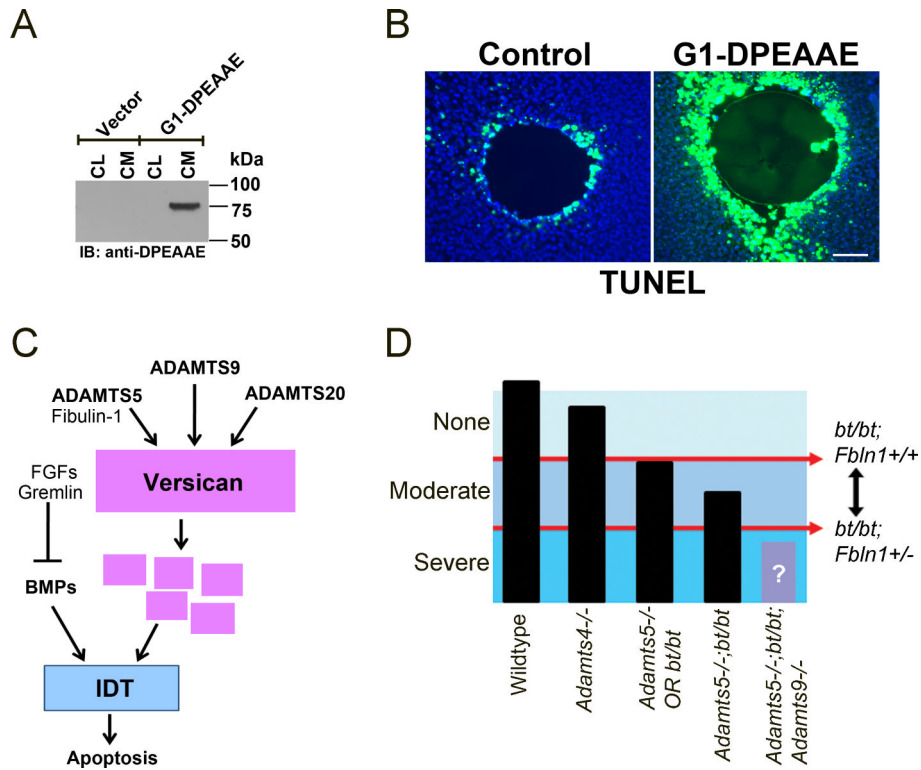
Figure 7. Versican G1-DPEAAE^{441} fragment induces apoptosis
A. Western blotting shows production and secretion of the G1-DPEAAE^{441} fragment in conditioned medium (CM) of stably transfected cells. The absence of immunoreactivity in cell lysate (CL) may reflect the relative abundance of accumulated G1-DPEAAE^{441} fragment in CM. **B**. A bead soaked in G1-DPEAAE^{441} fragment induced greater apoptosis over a wider distance compared to the control bead. The result is representative of six independent experiments for both the G1-DPEAAE^{441} fragment and control media. **C**. A proposed model for the role of ADAMTS proteases and versican in IDT regression, suggesting that ADAMTS-generated versican fragments may work synchronously with BMPs and create a permissive environment for BMP induction of apoptosis. **D**. Cooperative model of ADAMTS action. Cooperative maintenance of the required threshold of versican proteolysis is provided by spatial and temporal overlap of versican-degrading ADAMTS proteases in the IDT. Because two additional versican-degrading proteases (*Adamts1* and *Adamts9)* are implicated, we speculate on the existence of a second threshold below which more severe syndactyly, or STS affecting all web spaces may be seen (gray bar). Alteration of the level of fibulin-1 alters the proteolytic threshold by reducing ADAMTS5 activity.